



Metal-rich organic matter and hot continental passive margin: drivers for Devonian copper-cobalt-germanium mineralization in dolomitized reef-bearing carbonate platform

Nicolas J. Saintilan¹ · Corey Archer¹ · Colin Maden¹ · Elias Samankassou² · Stefano M. Bernasconi³ · David Szumigala⁴ · Zach Mahaffey⁴ · Andy West⁴ · Jorge E. Spangenberg⁵

Received: 10 November 2021 / Accepted: 26 April 2022 / Published online: 1 June 2022

© The Author(s) 2022

Abstract

The abundance and types of reef-bearing carbonate platforms reflect the evolution of Devonian climate, with conspicuous microbial-algal reefs in the warm Early and Late Devonian and sponge-coral reefs in the cooler Middle Devonian. A dolomitized Wenlock-Lower Devonian microbial-algal reef-bearing carbonate platform hosts epigenetic copper-cobalt-germanium (Cu-Co-Ge) sulfide mineralization at Ruby Creek-Bornite in the Brooks Range, Alaska. Here, we present rhenium-osmium (Re-Os) radiometric ages and molybdenum and sulfur ($\delta^{98/95}\text{Mo} = +2.04$ to $+5.48\%$ and $\delta^{34}\text{S} = -28.5$ to -1.8%) isotope variations for individual Cu-Co-Fe sulfide phases along the paragenetic sequence carrollite-bornite-pyrite. In the context of a hot, extensional passive margin, greenhouse conditions in the Early Devonian favored restriction of platform-top seawater circulation and episodic reflux of oxidized brines during growth of the carbonaceous carbonate platform. Molybdenum and sulfur isotope data signal the stepwise reduction of hot brines carrying Cu during latent reflux and geothermal circulation for at least ca. 15 million years from the Early Devonian until Cu-Co sulfide mineralization ca. 379–378 million years ago (Ma) in the Frasnian, Late Devonian (weighted mean of Re-Os model ages of carrollite at 379 ± 15 Ma [$n = 4$]; Re-Os isochron age of bornite at 378 ± 15 Ma [$n = 6$]). On the basis of petrographic relationships between sulfides and solid bitumen, and the Mo and S isotope data for sulfides, we imply that the endowment in critical metals (e.g., Co, Ge, Re) in the Ruby Creek-Bornite deposit is linked to the activity of primary producers that removed trace metals from the warm Early Devonian seawater and concentrated Co, Ge, and Re in algal-bacterial organic matter in carbonate sediments.

Keywords Rhenium-osmium · Bornite · Molybdenum · Algae · Bio-assimilated critical metals

Editorial handling: D. Dolejs

✉ Nicolas J. Saintilan
nicolas.saintilan@erdw.ethz.ch

¹ Institute of Geochemistry and Petrology, ETH Zürich, Clausiusstrasse 25, 8092 Zurich, Switzerland

² Department of Earth Sciences, Rue des Maraîchers 13, 1205 Geneva, Switzerland

³ Geological Institute, ETH Zürich, Sonneggstrasse 5, 8092 Zurich, Switzerland

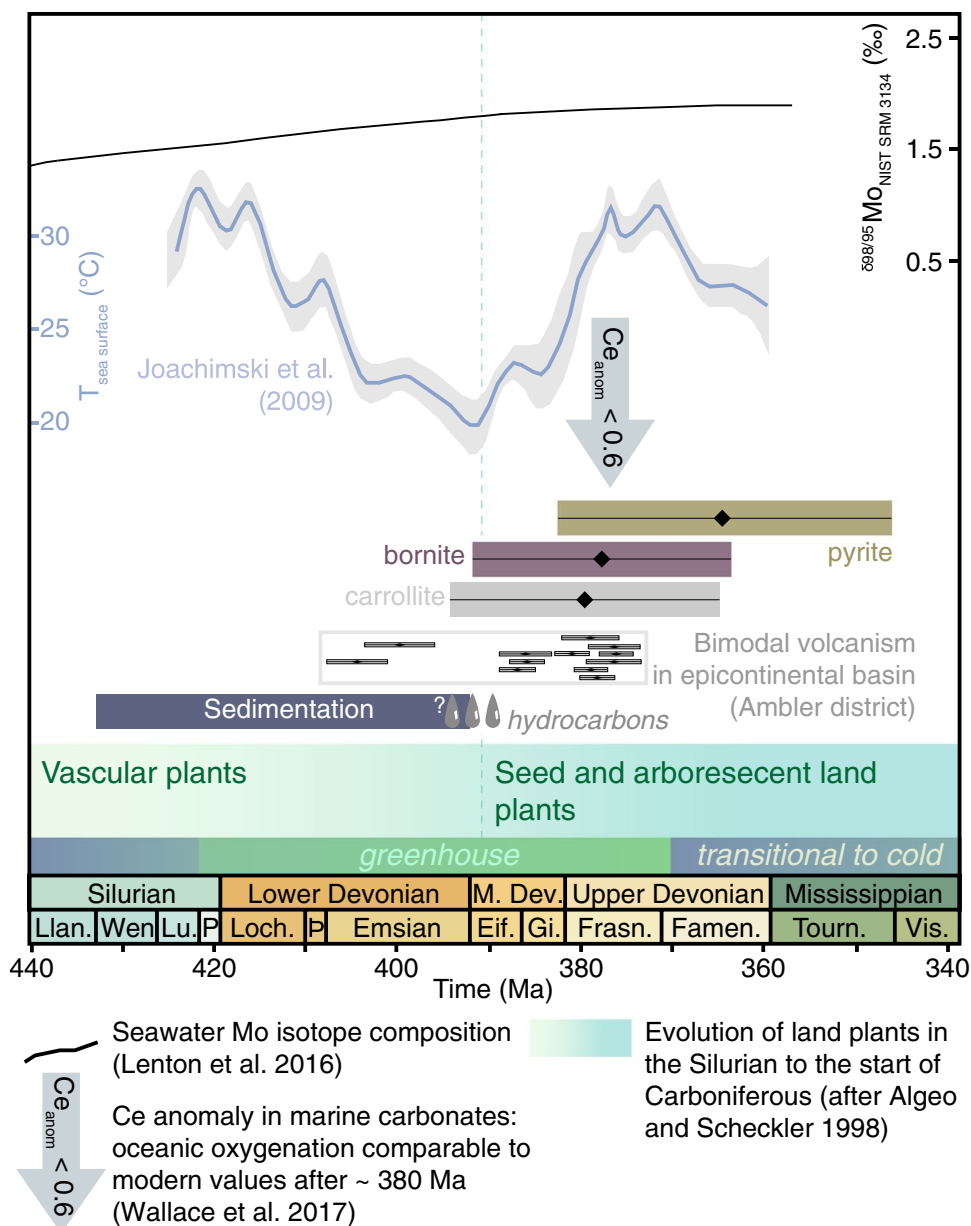
⁴ Ambler Metals LLC, 3700 Centerpoint Drive, Ste. #101, Anchorage, AK, USA

⁵ Institute of Earth Surface Dynamics, University of Lausanne, Building Geopolis, 1015 Lausanne, Switzerland

Introduction

The Devonian period was a warm greenhouse interval (Joachimski et al. 2009) that witnessed the largest reef constructions in Earth history (Copper and Scotese 2003) and the colonization of land plants (Algeo and Scheckler 1998; Lenton et al. 2016; Wallace et al. 2017; Fig. 1). The Devonian reef record reflects the evolution of Devonian climate (Joachimski et al. 2009). With warm to very warm sea surface temperatures in the Early and Late Devonian (Joachimski et al. 2009; Brugger et al. 2019), microbial-algal reefs were latitudinally widespread, i.e., 40°N to 46°S in the Lochkovian (416–411 Ma) and 45°N to 38°S in the late Frasnian-Famennian (377–359 Ma). Conversely, coral-stromatoporoid sponge reefs formed during the cooler Middle Devonian in water with intermediate tropical sea surface

Fig. 1 Chronology of stages of copper-cobalt (Cu-Co) mineralization at Ruby Creek-Bornite (new Re-Os isochron and model ages, this study; see ESM Fig. 1) in dolomitized carbonaceous limestone in a hot passive margin setting in the global context of ocean oxygenation and the rise of land plants in the Devonian (after Algeo and Scheckler 1998; Lenton et al. 2016; Wallace et al. 2017)



temperatures (Joachimski et al. 2009). Here, we focus on a dolomitized Wenlock-Lower Devonian microbial-algal reef-bearing carbonate platform in the Cosmos Hills, Southern Brooks Range, Alaska, USA (Fig. 2a and inset). This platform is host to the Ruby Creek-Bornite (RCB) copper-cobalt-germanium (Cu-Co-Ge) sulfide deposit associated with dolomite and post-oil solid bitumen (Hitzman 1986; Fig. 2b-k). In the context of reef expansion in the Devonian, we view the RCB deposit as a potential archive of the loops and feedbacks in the co-evolution of solid Earth, climate, and biosphere impacting on the flux of metals in the continental crust. Thus, this study is designed to explore the

timing, origin, and source of metals in the RCB deposit in the greater context of the Devonian greenhouse world. To this end, we used (1) rhenium-osmium (Re-Os) isotope geochronology of individual sulfide species, and (2) transition metal abundances and molybdenum isotope composition and (3) sulfur isotope composition of those same sulfide species. Our interpretations focus on (1) the first-order controls on the flow, pulses, and redox evolution of mineralizing basinal brines, and (2) the specific metal endowment of the RCB deposit in critical metals (e.g., Co, Ge, Ni) as a consequence of the breakdown of metal-rich algal-bacterial organic matter during dolomitization and sulfide mineralization.

Geological context and geodynamic setting in the Late Silurian to Late Devonian

The Scandian phase of the northern evolution of the Caledonian orogeny marked the final collision between Baltica and Laurentia (Miller et al. 2011; Gee et al. 2013; Robinson et al. 2019; Fig. 3a). At the end of convergence heralded by the Caledonian collision, a basin-and-range style of evolution commenced (Robinson et al. 2019). The Middle to Late Devonian rifting scenario involved crustal extension, thinning of the lithosphere, and incorporation of rift-related basin detritus in mantle-derived magmatism, as shown by zircon petrochronology (Miller et al. 2011; Hoiland et al. 2017; Robinson et al. 2019). Widespread extension triggered the opening of an epicontinental basin riddled by Middle to Late Devonian bimodal volcanism and associated granitic batholiths (Hitzman et al. 1986; Fig. 3a and 3b). This geodynamic configuration resulted in the opening of the Angayucham Ocean outboard of this northwest-facing epicontinental basin throughout the end of the Paleozoic and early Mesozoic (Hoiland et al. 2017; Robinson et al. 2019; Fig. 3a and 3b). A reef-bearing carbonate platform was built on a horst between the incipient Angayucham Ocean and this epicontinental basin on the seaboard of the extensional margin in Late Silurian (Wenlock—ca. 433 to 427 Ma) to Early Devonian (Emsian—ca. 407 to 393 Ma; Hitzman 1986; Hitzman et al. 1986; Till et al. 2008). Metazoan reefs rich in photozoans attest of shallow-marine water conditions in shelf zone with platform-top seawater circulation. Sustained warm air and sea surface temperatures (estimates of $T_{\text{air surface}} \geq 23 \text{ }^\circ\text{C}$ and $T_{\text{sea surface}} = \text{ca. } 19\text{--}29 \text{ }^\circ\text{C}$, at ca. 415 Ma and 40°N latitude; $T_{\text{air surface}} \geq 28 \text{ }^\circ\text{C}$ and $T_{\text{sea surface}} = \text{ca. } 29 \text{ }^\circ\text{C}$, at ca. 380 Ma and 20°N latitude; Joachimski et al. 2009; Brugger et al. 2019) favored carbonate reef building (Copper and Scotese 2003) in evaporitic sabkha setting on the edge of a shale-filled basin between 40°N latitude in the Late Silurian and 20°N latitude by the Late Devonian (Fig. 3a and 3b; Hitzman 1983, 1986; Hitzman et al. 1986; Till et al. 2008; Rohr et al. 2018; Robinson et al. 2019).

The Ruby Creek-Bornite deposit

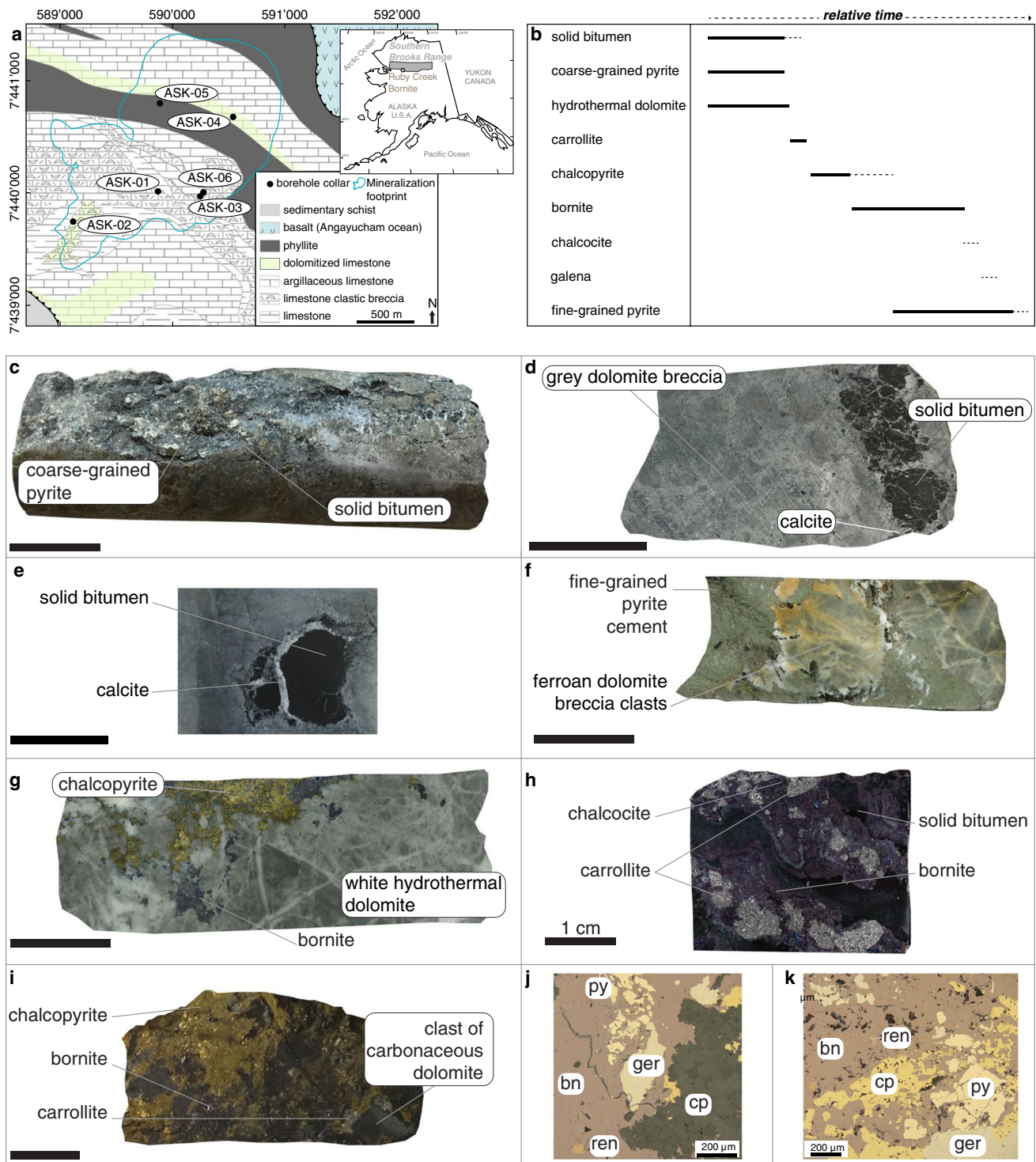
Geology and mineral characteristics of a carbonate-hosted Cu-Co-Ge ore deposit

The RCB Cu-Co-Ge sulfide deposit is located in the Ambler Mining District on the southern flank of the Brooks Range of Alaska, USA (Fig. 2a and inset). The RCB deposit is a large carbonate-hosted Cu-Co-Ge sulfide deposit with indicated copper resources of 41.7 million tons (Mt) at an average grade of 1.04% Cu, with an additional inferred resource of

144.1 Mt at an average grade of 1.68% Cu. The inferred cobalt resource amounts to 185.8 Mt at an average grade of 0.02% Co (Sim et al. 2022). In comparison, at the Kipushi Cu-Co-Ge deposit in the Central African Copperbelt, to which the RCB deposit was compared (Hitzman 1986; see below), the mined orebodies contained 60 Mt grading 11.0% Zn, 6.8% Cu, and 0.3% Ge (Intiomale and Oosterbosch 1974; Tshileo et al. 2003; Heijlen et al. 2008).

The RCB deposit is hosted by dolomitized Wenlock-Lower Devonian carbonate rocks incorporated in the Brooks Range fold-and-thrust-belt resulting from Jurassic to Cretaceous deformation (Hoiland et al. 2017, 2018). Unlike other parts of the Cosmos Hills subjected to greenschist-facies metamorphism at $114 \pm 5 \text{ Ma}$ (U–Pb zircon laser ablation inductively coupled mass spectrometry; Hoiland et al. 2018), the rocks hosting the RCB mineralization underwent limited metamorphic overprint, brittle disruption and preserve the record of hydrothermal events (Hitzman 1986). The conodont alteration index of 5–6 suggests that temperature in the carbonate rocks remained below $360 \text{ }^\circ\text{C}$ (Till et al. 2008) throughout their geodynamic evolution. The rocks hosting the RCB deposit show an inward zonation from the outer carbonaceous limestone to a halo of low iron dolomite with disseminated and intergranular solid bitumen (Fig. 2c–e, “Dolomites A & B”, see below), around a core of ferroan dolomite (Fig. 2f) with intergranular solid bitumen. A fault-controlled and retreating hydrothermal front drove patchy dolomitization promoted by oxidation of organic matter and shaped by internal argillaceous limestone aquitards (i.e., “seals”) during early and burial diagenesis (Hitzman 1986). This pattern is compatible with multiple pulses of Fe–Mg-rich acidic hydrothermal fluids involved in (1) fluid-rock interaction and alteration of organic compounds (mainly hydrocarbons) increasing the dissolved inorganic carbon content, (2) dissolution and recrystallization of earlier dolomite phases up to $300 \text{ }^\circ\text{C}$, and then (3) hydraulic brecciation in dolostone of low ductility (Hitzman 1986; Davies and Smith 2006; Fig. 2g).

Disseminated, fine-grained pyrite started mineralizing early in the paragenetic sequence (Bernstein and Cox 1986). An initial and pervasive dolomite that includes disseminated solid bitumen in intergranular voids and stylolites (“Dolomite A” of Hitzman 1986) overlies the most abundant dolomite facies in the mineralization (“Dolomite B” of Hitzman 1986). The latter occurs as irregular veins and breccias including clasts of dolomite A. Fine-grained pyrite is ubiquitous in dolomite B and most abundant at the gradational contact with dolomite A. Solid bitumen is coarse in dolomite B and fills intergranular voids (Hitzman 1986). The origin and crucial role of this organic matter in the mineralizing processes are discussed in the present work on the basis of the new petrographic and isotope data combined with



previous interpretations by Runnells (1965) and Hitzman (1986).

Above the core of ferroan dolomite, massive bornite ± chalcocite-calcite mineralization is commonly located at the lower contacts of the shale aquitards in the low-iron dolomite B. Bornite-mineralized zones replaced massive coarse-grained, cobaltiferous pyrite with minor

sphalerite that had formed below, and around, the shale aquitards. Those bornite-rich zones are surrounded by haloes of chalcocite-bornite-calcite ± dolomite ± carrollite (Cu[Co,Ni]₂S₄). Hydraulic brecciation of dolomite resulted in additional copper mineralization in the form of a dense network of bornite ± chalcocite-white dolomite-mineralized veins and stringers that cut across the ferroan

Fig. 2 **a** Geological map of the Cosmos Hills in the area of the Ruby Creek-Bornite (RCB) Cu-Co deposit (source: Ambler Metals LLC and after Till et al. 2008) as well as its location in Northern Alaska (inset). The currently known footprint (~2,500 m×1,500 m) of the deposit is projected to surface. The collars of the boreholes from which samples ASK-01 to ASK-06 were collected and analyzed in the present study are shown. See ESM Table 1 for a list and geographical information of the samples. **b** Paragenetic sequence at the Ruby Creek-Bornite deposit based on the studied samples. **c–e** Grey, clast-supported dolomite breccia is impregnated by solid bitumen as clots or films with haloes of white calcite. Solid, black to dark brown solid bitumen (insoluble in organic solvents) may be intergrown with coarse-grained subhedral to euhedral pyrite. **f** Fine-grained pyrite (sample ASK-02), which is in part coeval with bornite precipitation and may be distributed in the outer zones of RCB, cemented breccia of rounded and sub-angular clasts of ferroan dolomite associated with barium silicates. **g** Veins of and disseminated bornite and chalcopyrite, locally replaced angular clasts of light grey to white hydrothermal dolomite (ASK-05). The latter resulted from hydraulic brecciation of earlier grey dolomite, including veinlets in anastomosing networks. Brecciation and veining preceded and were coeval with chalcopyrite and bornite. **h, i** Coarse-grained grey carrollite ($\text{Cu}[\text{Co},\text{Ni}]_2\text{S}_4$) cemented solid bitumen and clasts of dolomitized carbonaceous limestone before cementation by chalcopyrite and/or bornite with accessory chalcocite. Carrollite could have formed from the breakdown of pyrite (Hitzman 1986), associated with organic matter in carbonaceous limestone (ASK-06 and ASK-03). **j, k** Germanite ($\text{Cu}_{13}\text{Fe}_2\text{Ge}_2\text{S}_{16}$) after chalcopyrite, extensively replaced by bornite. Renierite ($\text{Cu}_{11}\text{Ge}_2\text{Fe}_4\text{S}_{16}$) as <100- μm -large clots disseminated in bornite where the latter is intimately associated with solid bitumen and/or carbonaceous dolomite (reflected light microphotographs from Fig. 2i). Unless specified all scale bars are 2 cm long. Abbreviations: py: pyrite, bn: bornite, ger: germanite, ren: renierite, cp: chalcopyrite

and low iron dolomites (Fig. 2g), and even locally into the non-dolomitized carbonaceous limestone (Hitzman 1986).

Tennantite-tetrahedrite are closely associated with chalcopyrite and rarely found in bornite-rich zones. Anhedral grains of tennantite-tetrahedrite are intergrown with chalcopyrite in millimetre-thick veinlets (Bernstein and Cox 1986). Contrary to tennantite-tetrahedrite, zinc-bearing renierite ($\text{Cu}_{10}\text{ZnGe}_2\text{Fe}_4\text{S}_{16}$) and germanite ($\text{Cu}_{13}\text{Fe}_2\text{Ge}_2\text{S}_{16}$) are found almost exclusively in association with, and as inclusions in, bornite (Fig. 2j, k). Arsenian renierite ($\text{Cu}_{11}\text{GeAsFe}_4\text{S}_{16}$) and vanadium-bearing germanite (with up to 3 wt% V) are specific to the RCB deposit (Bernstein and Cox 1986).

Cymrite, a micaceous barium silicate ($\text{BaAl}_2\text{Si}_2(\text{O},\text{OH})_8\cdot\text{H}_2\text{O}$), is found as sheet-like crystals (1–2 vol%) with pseudomorphs of copper sulfides (Runnells 1964, 1969). Cymrite is most abundant in the core of iron-rich dolomite which is bereft of significant copper mineralization. The presence of Ba-silicate and the absence of abundant barite in the deposit with only rare deposition of barite late in the paragenetic sequence after copper sulfides (Runnells 1969) signals late availability of sulfate in the system.

Is the RCB deposit unique?

The RCB deposit shares striking similarities with the Kipushi Cu-Co-Ge sulfide deposit in the Central African Copperbelt (Heijlen et al. 2008) and the Otavi Mountain Land district (including the Tsumeb Cu deposit) in Namibia (Chetty and Frimmel 2000). These large deposits have in common (1) features of diagenetic to epigenetic sulfide mineralization, (2) emplacement in carbonate stratigraphy, and (3) early pyrite-dolomite alteration of the host limestone followed by copper dominant sulfide mineralization. All these deposits occur in intra-continental to continental margin settings characterized by extensional tectonics and bimodal volcanism (Chetty and Frimmel 2000; Hitzman et al. 2010). Basin-margin faults seem to play an important role in localizing mineralizing fluids (Hitzman et al. 2010). Yet, the canonical interpretation of lithological break as syn-sedimentary faults was recently challenged (Turner et al. 2018; Spinks et al. 2021). Lithological breaks associated with sulfide mineralization were reinterpreted at Kipushi as steep depositional margin of carbonate lithofacies where carbonate build-up focused mineralizing fluids when in contact with overlying fine-grained terrigenous strata (e.g., shale and siltstone aquitards; Turner et al. 2018). The critical control of carbonate lithofacies is highlighted further at the RCB and Kipushi deposits where the Cu-Co-Ge sulfide orebodies are intimately associated with solid bitumen in dolomite (Runnells 1964, 1965, 1969; Hitzman 1986; Heijlen et al. 2008). Given this detailed knowledge for carbonate-hosted Cu-Co-Ge deposits, our present study explores the controls exerted on the mineralizing processes at Ruby Creek-Bornite by (1) a hot continental passive margin setting and (2) the chemical and redox potential of carbonaceous limestone in a reef-bearing platform on this continental margin. Our goal is to contribute advances that can be utilized to build a greater understanding of the origin of Ruby Creek-Bornite-Kipushi-type ore deposits.

Results

Paragenetic relationships of sulfides, solid bitumen, and dolomite

Detailed ore textures and mineralogy are provided in Runnells (1969) and Hitzman (1986). The petrographic observations and paragenetic relationships (Fig. 2b–k) presented here pertain to the samples that were used to contextualize the new sulfide-specific radiogenic and stable isotope data. Grey, clast-supported dolomite breccia is impregnated by solid bitumen as coalesced clots and globules, or films with haloes of white calcite (Fig. 2c–e). Solid, black to dark

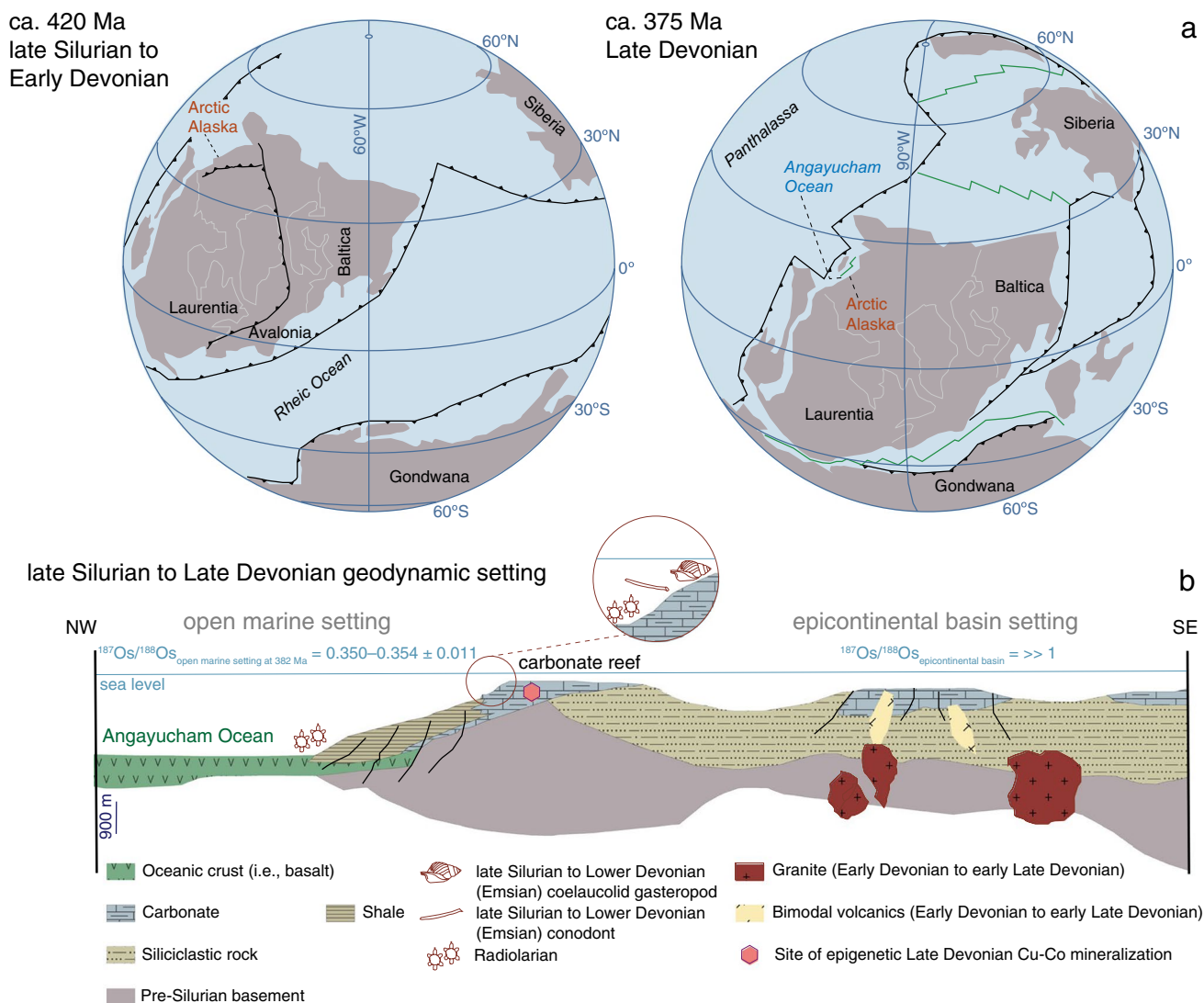


Fig. 3 **a** Plate reconstruction and paleogeography of Alaska from the Late Silurian to the Late Devonian (after Robinson et al. 2019). **b** Paleogeodynamic setting of the Ambler district as an epicontinental

basin at the time of opening of the Angayucham Ocean at ca. 375 Ma (after Hitzman et al. 1986)

brown solid bitumen (insoluble in organic solvents) may be intergrown with coarse-grained subhedral to euhedral pyrite (Fig. 2c). Fine-grained pyrite (sample ASK-02), which is in part coeval with bornite precipitation and may be distributed in the outer zones of RCB, cements breccia of rounded and sub-angular clasts of ferroan dolomite associated with barium silicates (Fig. 2f). Veins and disseminated bornite and chalcopyrite cement and locally replace angular clasts of light grey to white hydrothermal dolomite (sample ASK-05). The latter resulted from hydraulic brecciation of earlier grey dolomite, including veinlets in anastomosing networks. Brecciation and veining preceded and were coeval with chalcopyrite and bornite (Fig. 2g). Coarse-grained grey carrollite cemented solid bitumen and clasts of dolomitized

carbonaceous limestone before cementation by chalcopyrite and/or bornite with accessory chalcocite (samples ASK-06 and ASK-03; Fig. 2h and i). In these sulfide-rich samples associated with solid bitumen and clasts of carbonaceous limestone, germanite, which formed coevally with and after chalcopyrite, was included and locally replaced by bornite (Fig. 2j and k). In those same samples, renierite is found as < 100- μm -large clots that are disseminated in bornite.

Radiogenic and stable isotope geochemistry of Late Devonian sulfides We complement a preliminary Re-Os date (384 ± 4 Ma) produced by using data points of multiple sulfide phases (bornite, chalcopyrite, pyrite from ore dump samples) in a single isochron regression in the ^{187}Re versus

^{187}Os space (i.e., by considering an initial [$^{187}\text{Os}/^{188}\text{Os}$]_i ratio of 0.3 ± 5.5 ; Selby et al. 2009). Here, we use the new method of Re–Os isotope geochemistry and isochron regression applied to mineral separates of individual sulfide species co-existing in single hand samples (carrollite, bornite, pyrite in this paragenetic order; Fig. 2b, Electronic Supplementary Materials—ESM Table 1) but analyzed separately (Saintilan et al. 2018, 2020). The $\delta^{34}\text{S}$ signatures of these mineral separates were constrained by standard techniques whereas variations in the $\delta^{98/95}\text{Mo}$ of purified Mo fractions of each sulfide species were determined by multicollector inductively coupled mass spectrometry. Extended methods, explanation of data handling, and diagrams of Re–Os isochron and model ages are provided in the ESM.

Rhenium and total Os (Os_{total}) concentrations in the analyzed sulfides are high (59.2 to 642.4 ng g⁻¹ and 274 to $2,933$ pg g⁻¹, respectively; Table 1). Common Os contents, estimated using abundances in ^{192}Os , represent a negligible fraction of Os_{total} (11 to 113 pg g⁻¹ ^{192}Os). The elevated $^{187}\text{Re}/^{188}\text{Os}$ values ($9,615$ – $13,521$) that are positively correlated with highly radiogenic $^{187}\text{Os}/^{188}\text{Os}$ ratios (59.3 – 87.5) are diagnostic of a total ^{187}Os budget that largely comprises radiogenic $^{187}\text{Os}^*$ (95.0 – 98.8%) with minor correction for common $^{187}\text{Os}_{\text{c}}$. Carrollite (527.5 – 642.4 ng g⁻¹ Re; $2,429$ – $2,933$ pg g⁻¹ Os_{total} ; 36.9 – 61.1 μg g⁻¹ Mo; Tables 1 and 2) and bornite (393.7 – 472.3 ng g⁻¹ Re; $1,735$ – $2,135$ pg g⁻¹ Os_{total} ; 21.3 – 28.9 μg g⁻¹ Mo) cementing solid bitumen and fragments of carbonaceous limestone (Fig. 2h, i) have the highest Re, Os_{total} , and Mo contents. The sulfides span a large range of isotopically heavy Mo isotope compositions with carrollite ($+3.78$ to $+3.89\%$) and bornite ($+2.21$ to $+5.49\%$) being isotopically heavier than pyrite ($+2.04$ to $+2.24\%$; Table 2 and ESM Table 2).

Preserved Re–Os systematics of six bornite aliquots ($\delta^{34}\text{S} = -28.5 \pm 0.4\%$ to $-2.8 \pm 0.5\%$; Table 2) yield a Model 3 Re–Os isochron date of 378 ± 15 Ma that accounts for potential variability in the initial $^{187}\text{Os}/^{188}\text{Os}$ (Os_i) of each aliquot within the 2.40 ± 2.86 range determined by isochron regression (ESM Fig. 1). These bornite aliquots have individual model ages at ca. 379–376 Ma whereas three additional aliquots of bornite that are positioned slightly above ($\delta^{34}\text{S} = -7.8 \pm 0.3\%$) and below ($\delta^{34}\text{S} = -3.6 \pm 0.3\%$) the 378-Ma isochron have slightly older (ca. 385 Ma) and younger (ca. 364 Ma) model ages, respectively. The Re–Os data of single carrollite aliquots ($n=4$; $\delta^{34}\text{S} = -1.8 \pm 0.4\%$) return model ages between 383 and 375 Ma and a weighted mean average at 379 ± 15 Ma. Similarly, individual aliquots of fine-grained pyrite cement ($n=3$; $\delta^{34}\text{S} = -2.7 \pm 0.3\%$) have Re–Os data yielding model ages between 367 and 354 Ma and a weighted mean average at 364 ± 18 Ma (ESM Fig. 1).

Discussion and conclusions

Large-scale fluid flow and tectonic controls on Late Devonian mineralization

In the extensional tectonic setting of a carbonate shelf at the margin of an epicontinental basin (Fig. 3b), basin dewatering contributed active reflux of fluids derived from evaporitic brines in the host reefal, Wenlock to Emsian carbonate platform (Hitzman 1986). With high heat flow sustained by bimodal volcanic activity in the adjacent epicontinental basin from ~ 405 to 376 Ma (U–Pb zircon geochronology; McClelland et al. 2006; Raterman et al. 2006; Figs. 1 and 3b), brine-derived fluids then circulated via a combination of latent reflux (Jones et al. 2002) and geothermal circulation for at least 15–30 million years from the late Emsian to ca. 379–364 Ma (Re–Os time stamps for Cu–Co sulfide mineralization, including pyrite; Fig. 1). The brine fluids with salinities at 7 to 13 wt% eq. NaCl (2 to 4 times average Cambrian–Devonian seawater salinity; Demicco et al. 2005) could produce matrix dolomite at temperatures as high as 300 °C and then cooled to precipitate Cu sulfides at ~ 120 – 225 °C (Hitzman 1986). Molybdenum isotope variations in sulfides with high Mo contents (3.3 to 61.1 μg g⁻¹ Mo) trace the hydrological cycle of brine fluids encountering an increasingly anoxic environment (Ryb et al. 2009), until formation of reduced sulfide-bearing and copper-rich fluids (Fig. 4). The conditions, which led to the involvement of reduced sulfide-bearing and copper-rich fluids in the mineralizing processes, are explained below. In brines derived from Mo-rich (> 50 μg g⁻¹) Devonian seawater (Scott et al. 2008; $\delta^{98/95}\text{Mo}_{\text{seawater}} = +1.84 \pm 0.10\%$; Gordon et al. 2009), Mo remains in solution as molybdate [MoO_4^{2-}] under oxic conditions (Ryb et al. 2009). The progressive and incomplete sulfidation of [MoO_4^{2-}] to tetrathiomolybdate [MoS_4^{2-}] in brine is accompanied by net residual fluid positive isotope fractionation during subsurface brine migration (Ryb et al. 2009; Kerl et al. 2017). This process is recorded in the Mo isotope composition of the pyrite cement (8 – 10 μg g⁻¹ Mo; $\delta^{98/95}\text{Mo} = +2.04$ to $+2.24\%$; Fig. 4) of ferroan dolomite that precipitated at ca. 364 Ma once the geothermal gradient was insufficient for brines to be hot enough to transport copper in solution. These temporal and geochemical constraints imply that the hydrological cycle evolved in space and time with the earlier inflow of reduced sulfide-bearing and copper-rich brines at ca. 379–378 Ma (Fig. 4) that caused hydraulic fracturing and cementation of angular to sub-angular fragments of matrix dolomite by white hydrothermal dolomite and Cu–Co sulfides (Fig. 2g). By consuming isotopically heavy MoS_4^{2-} complexes in subsurface reducing conditions, bornite precipitated with heavy Mo isotope signatures ($\delta^{98/95}\text{Mo} = +2.21$ to $+2.75\%$;

Table 1 Synopsis of the Re-Os isotope geochemistry data for bornite, carrollite, and pyrite at Ruby Creek-Bornite, Southern Brooks Range, AK

Name	Min- eral	Ali- quot size (mg)	Re (ng/g)	± 2 s Re (ng/g)	^{187}Re (ng/g)	± 2 s ^{187}Re (ng/g)	Total Os (pg/g)	± 2 s Total Os (pg/g)	^{192}Os (pg/g)	± 2 s ^{192}Os (pg/g)	$^{187}\text{Os}^*$ (pg/g)	± 2 s $^{187}\text{Os}^*$ (pg/g)	(%)	$^{187}\text{Os}/^{188}\text{Os}$ ± 2 s	ρ	% R_{blk}	% $^{187}\text{Os}_{\text{blk}}$	% $^{188}\text{Os}_{\text{blk}}$	Os_i at isochron age ^a	± 2 s	Model age ^b (Ma)	± 2 s			
004-01- ASK-01	Bornite	53.10	142.89	0.20	89.81	0.13	649	7	26.6	0.1	564	41	96.3	10,694	36	69.7	0.4	0.520	0.021	0.016	0.858	2.35	0.45	377	32
007-01- ASK-01	Bornite	55.74	146.16	0.16	91.86	0.10	662	7	26.1	0.1	578	40	96.5	11,139	41	72.7	0.4	0.614	0.015	0.007	1.176	2.53	0.48	378	31
008-01- ASK-01	Bornite	54.89	142.13	0.19	89.34	0.12	643	6	25.7	0.1	561	39	96.4	10,985	32	71.5	0.3	0.559	0.042	0.007	1.211	2.31	0.37	377	31
004-03- ASK-03	Bornite	80.89	452.01	0.52	284.11	0.32	2,042	17	76.7	0.1	1,797	117	96.6	11,721	25	76.7	0.3	0.429	0.004	0.003	0.197	2.87	0.33	379	29
006-03- ASK-03	Bornite	59.00	472.27	0.64	296.84	0.40	2,135	20	80.2	0.2	1,878	123	96.6	11,709	35	76.7	0.3	0.560	0.006	0.007	0.179	2.89	0.41	379	29
008-04- ASK-04	Bornite	62.13	98.12	0.11	61.67	0.07	433	5	14.4	0.1	387	22	97.1	13,521	54	87.5	0.5	0.694	0.054	0.010	1.894	2.27	0.59	376	25
005-08- ASK-06	Bornite	59.55	403.31	0.59	253.49	0.37	1,774	20	73.9	0.3	1,538	113	96.2	10,856	44	68.4	0.4	0.591	0.007	0.005	0.277	0.03	0.50	364	32
007-06- ASK-06	Bornite	57.97	393.71	0.41	247.46	0.26	1,735	15	72.6	0.2	1,504	111	96.2	10,793	27	68.1	0.3	0.599	0.005	0.003	0.410	0.41	0.15	364	32
005-06- ASK-05	Bornite	75.59	59.21	0.16	37.22	0.10	274	5	10.9	0.2	239	18	96.4	10,784	180	71.8	2.1	0.552	0.036	0.026	1.458	3.86	2.40	385	33
006-02- ASK-02	Pyrite	70.26	248.04	0.30	155.90	0.19	1,103	6	47.0	0.1	947	81	95.6	10,505	17	66.8	0.1	0.410	0.009	0.011	0.256	n.a	n.a	367	32
007-02- ASK-02	Pyrite	75.14	324.16	0.26	203.75	0.17	1,414	13	52.1	0.2	1,241	90	96.2	12,385	36	78.4	0.4	0.619	0.005	0.002	0.441	n.a	n.a	367	28
008-02- ASK-02	Pyrite	56.85	220.56	0.23	138.63	0.14	964	7	45.6	0.1	813	79	95.0	9,615	21	59.3	0.2	0.558	0.026	0.005	0.663	n.a	n.a	354	36
006-05- ASK-06	Carrol- lite	57.55	642.40	0.87	403.77	0.55	2,933	28	113.3	0.3	2,632	234	98.8	11,276	35	74.4	0.4	0.569	0.004	0.005	0.130	n.a	n.a	382	30
006-06- ASK-06	Carrol- lite	62.31	527.54	0.68	331.57	0.42	2,429	17	97.8	0.2	2,169	202	98.8	10,728	23	71.1	0.2	0.527	0.005	0.006	0.139	n.a	n.a	383	32
008-06- ASK-06	Carrol- lite	62.21	548.15	0.55	344.53	0.35	2,478	17	101.4	0.2	2,209	209	98.8	10,758	19	69.8	0.2	0.531	0.010	0.002	0.274	n.a	n.a	375	32
008-07- ASK-06	Carrol- lite	59.17	569.85	0.60	358.17	0.38	2,575	18	103.2	0.2	2,301	213	98.8	10,983	20	71.4	0.2	0.483	0.010	0.002	0.283	n.a	n.a	376	31

^aCalculated with a model age of 378 ± 15 Ma for bornite aliquots^bModel age calculated with correction for common Os using $^{187}\text{Os}/^{188}\text{Os}_{\text{(initial)}}$ of 2.40 ± 2.86 from the Model 3 isochron for bornite

n.a. not applicable

Table 2 Summary of the transition metal abundances (nickel and molybdenum) and molybdenum and sulfur isotope data for bornite, carrollite, and pyrite at Ruby Creek-Bornite, Southern Brooks Range, AK

Sample	Mineral	Petrographic texture	Sample weight (g)	Ni ($\mu\text{g g}^{-1}$)	Mo ($\mu\text{g g}^{-1}$)	$\delta^{34}\text{S}$ V-CDT ($\text{‰} \pm 2$ standard error)	$\delta^{98/95}\text{Mo}$ V-NIST- SRM3134 (Batch #1) (‰)
ASK-02a	Pyrite	Cement of ferroan dolomite	0.03714	138	8.1	-2.7 ± 0.3 ($n=2$)	+2.22
ASK-02b	Pyrite		0.07538	190	10.1		+2.13
ASK-06_CAR_a	Carrollite	Cementing solid bitumen and	0.07432	34,077	61.1	-1.8 ± 0.4 ($n=6$)	+3.78
ASK-06_CAR_b	Carrollite	fragments of dolomitized carbonaceous limestone	0.05320	69,063	36.9		+3.86
ASK-01	Bornite	Replacing coarse-grained pyrite and associated with solid bitumen	0.02899	1.3	13.9	-28.5 ± 0.4 ($n=3$)	+2.44
ASK-03	Bornite	Cementing solid bitumen and fragments of dolomitized carbonaceous limestone	0.02114	13.5	28.9	-3.3 ± 0.2 ($n=3$)	+5.48
ASK-04	Bornite	Associated with white hydrothermal dolomite and cementing clasts of dolomite matrix	0.02856	1.3	15.6	-2.8 ± 0.5 ($n=6$)	+2.75
ASK-05	Bornite	Associated with white hydrothermal dolomite	0.06387	0.14	3.3	-7.8 ± 0.3 ($n=2$)	+2.21
ASK-06_Bn	Bornite	Cementing solid bitumen and fragments of carbonaceous limestone	0.03934	123	21.3	-3.6 ± 0.3 ($n=2$)	+3.53

Fig. 4). The latter and the dominant sulfur isotope compositions of Cu-Co sulfides and pyrite in the RCB ($\delta^{34}\text{S} = -3.6$ to -1.8‰) are compatible with leaching of copper, sulfur, and additional isotopically heavy Mo from magmatic sulfides (Voegelin et al. 2012) in newly formed oceanic crust flooring the shale-filled basin adjacent to the carbonate platform. In this context, we suggest that high heat gradient conditioned the co-transport of copper and reduced sulfur species in solution at moderate temperatures (≥ 200 – 225 °C; Zhong et al. 2015). Furthermore, Cu-Co sulfides are present at the contact of solid residues of post-oil solid bitumen and coarse-grained pyrite in the dolomitized carbonaceous limestone (Fig. 2h, i). The interaction of relatively reduced, copper-rich brines with organic matter and additional precipitation of Cu-Co sulfides using isotopically light, biogenic hydrogen sulfide (Runnells 1969; $\delta^{34}\text{S} = -28.5$ to -7.8‰ , this study) explains an additional net residual fluid positive fractionation of Mo isotopes: the light Mo isotopes were scavenged by organic compounds (Ryb et al. 2009; King et al. 2018) resulting in the heaviest Mo isotope compositions in Cu-Co sulfides ($\delta^{98/95}\text{Mo}_{\text{bornite}} = +2.44$ to $+5.49\text{‰}$; $\delta^{98/95}\text{Mo}_{\text{carrollite}} = +3.78$ to $+3.89\text{‰}$; Fig. 4).

Our findings highlight the importance of ore-forming processes associated with brine-derived fluid flow in organic-rich carbonate lithofacies during the evolution of a Late Silurian to Devonian hot continental margin. In fact, a remarkable feature of the Devonian worldwide may be

that of ore-forming processes involving either (1) large-scale flow of heated evaporitic basinal brines, and/or (2) strong controls on sub-surface sulfidic conditions by the extent of organic carbon burial in continental margin (e.g., Mako and Shanks III 1984; Wilkinson et al. 2005; Magnall et al. 2018; Gadd et al. 2020; Saintilan et al. 2022). For the Late Devonian specifically, it is suggested that high primary productivity and enhanced organic carbon burial were key processes for sulfidic trap sites for metals in sub-surface conditions (Magnall et al. 2018). In the next section, we develop a model in which primary producers (Falkowski and Knoll 2011) in Early Devonian seawater acted as efficient metal traps. In this model, we further explain how organic carbon burial in platformal carbonaceous limestone not only optimized sub-surface sulfidic conditions, but also contributed to the metal endowment of the RCB deposit.

Supplementary biogenic metal source

Textural evidence suggests that solid bitumen is derived from tiny particles of organic matter that were endogenous to the carbonate sediments that lithified into the carbonaceous limestone hosting the RCB deposit (Runnells 1965). The positive spatial relationship between solid bitumen and recrystallized, clear dolomite (Fig. 2d, e) suggests that recrystallized dolomite results from the removal of tiny particles of black carbonaceous matter that coalesced into

liquid hydrocarbon endogenous to the host limestone. This process left recrystallized dolomite clear and commonly free of dust-size, finely disseminated carbonaceous matter (Runnells 1965; Hitzman 1986). The rarer type of solid bitumen, shaped like droplets, and filling vugs with a halo of white calcite (Fig. 2e; Runnells 1965; Hitzman 1986, this study) may represent areas where endogenous hydrocarbon flowed in liquid form into vugs within the host dolomite (Runnells 1965). In summary, all textural and geochemical evidence (Runnells 1965; Hitzman 1986, this study) favor a preferred interpretation that hydrocarbons were related to an endogenous source rather than hydrocarbons derived from a regional shale source rock. Runnells (1965) suggested that endogenous hydrocarbon moved in suspension in the basinal brines throughout dolomitization and sulfide mineralization.

In our model, we suggest that algal–bacterial organic matter endogenous to limestone not only contributed subsurface sulfidic conditions favorable for sulfide mineralization but also acted as a specific source of critical metals in the RCB deposit. Indeed, in light of petrographic evidence and our new $\delta^{98/95}\text{Mo}$ and $\delta^{34}\text{S}$ data, we propose that the high Re contents, the variable Os_i of Cu–Co sulfides, and the association of Ge–sulfides consistently with Cu–Co sulfides (Fig. 2) relate to algal–bacterial primary producers in the warm Early Devonian seawater. These micro-organisms fed on Re, Co, Ge, and minor Os as catalyzers in their metabolic pathways until incorporation of this metal-rich organic matter in carbonate sediments and lithification to carbonaceous limestone. In details, Ge can be bio-assimilated by modern microalgae in surface waters (Sutton et al. 2010). Modern microalgae and bacteria utilize Co and Ni as alternatives to elements essential to their metabolism (Andersson et al. 2020; Hawco et al. 2020; Morel et al. 2020). Modern macroalgae accumulate Re preferentially over Os from seawater. The abundance of Re (10s of ppb) and Os (100s of ppt) in macroalgae is primarily controlled by uptake from the dissolved load in local seawater (Racionero-Gómez et al. 2016, 2017). The Wenlock–Lower Devonian reef-bearing carbonate platform developed at the interface between open marine conditions ($^{187}\text{Os}/^{188}\text{Os}_{\text{seawater at 382 Ma}} \sim 0.350\text{--}0.354 \pm 0.011$; Fig. 3b; Saintilan et al. 2021) and an epicontinental basin under the influence of coastal inputs ($\text{Os}_{\text{basin-rivers}} > 1$; Peucker-Ehrenbrink and Ravizza 2000) combining the effects of erosion of the Caledonian orogen (Robinson et al. 2019) and the impact of land plants on chemical weathering of crustal sulfides and organic matter (Algeo and Scheckler 1998). Macroalgae do not fractionate Os isotopes and record variations in $^{187}\text{Os}/^{188}\text{Os}$ of seawater at the month to year scale (Racionero-Gómez et al. 2017). Therefore, we suggest that the high variability of the bornite Os_i (2.40 ± 2.86) is driven by original assimilation of Os by algae in the carbonate platform setting in the Devonian (Fig. 3b). In conclusion, we posit that the endowment in Co, Ge, and Re in the RCB

deposit results from elemental exchange at the micro-scale between the hot mineralizing fluids and algal–bacterial organic matter in carbonaceous limestone of high chemical potential.

Climax of Devonian greenhouse conditions in the Frasnian: a contribution to the flow of mineralizing fluids?

The age of the epigenetic Cu–Co sulfide mineralization at ca 379–378 Ma coincides with the ca. 380–375 Ma upslope to the climax of greenhouse climatic conditions in the Frasnian–Famennian (Fig. 1). We question whether this temporal overlap is a causal or a fortuitous relationship. In the context of a hot, extensional passive margin (Hitzman 1986; Hitzman et al. 1986), we discuss whether short-term transgression–regression pulses (Shalev and Yechieli 2007) in a warming Frasnian climate (Joachimski and Buggisch 2003; Joachimski et al. 2009) could have been an additional contribution to the up-and-down flux (Shalev and Yechieli 2007) of mineralizing brines in dolomitized carbonaceous limestone. Transgression–regression cycles induce “fluid pumping” that causes fluid pressure changes and modifies the flow of oxidized, evaporitic residual brines in marginal and rift basin (Vasyukova and Williams-Jones 2022), i.e., recession of sea level may cause brine discharge whereas rise of sea level makes brines sink through faults and migrate through tilted blocks (Shalev and Yechieli 2007).

The building of the reef-bearing carbonate platform that hosts the RCB deposit took place during a decline of sea level from the Late Silurian (Ludlow) through Early Devonian (Emsian) following a eustatic high in mid-Wenlock (Haq and Schutter 2008). The Middle Devonian coincided with the beginning of another long-term and continuous rise of sea level (Johnson et al. 1985), which reached its acme in the early Late Devonian (ca. 382 Ma; Frasnian; Haq and Schutter 2008). The timing of Cu–Co sulfide mineralization at ca. 379–378 Ma overlaps with the end of rapidly succeeding transgression–regression cycles that commenced at ca. 383 Ma (i.e., “depohase IIb” of Johnson et al. 1985) in this overall global transgression (Johnson et al. 1985; Kabanov and Jiang 2020). Under greenhouse conditions in the Late Devonian (Fig. 1), glacio-eustasy is non-existent and third-order sea level changes of 15–35 m in the Middle to Late Devonian are documented (Witzke 2011; Smith et al. 2019a, b; Kabanov and Jiang 2020) although sea-level changes up to 90–145 m from the late Middle Devonian (Givetian) to Late Devonian (Famennian) may have been possible (Witzke 2011; Ver Straeten et al. 2019). Therefore, in this context and considering the “fluid pumping” model (Shalev and Yechieli 2007; Vasyukova and Williams-Jones 2022), we conceptualize that succeeding transgression–regression cycles at the climax of Devonian greenhouse conditions may

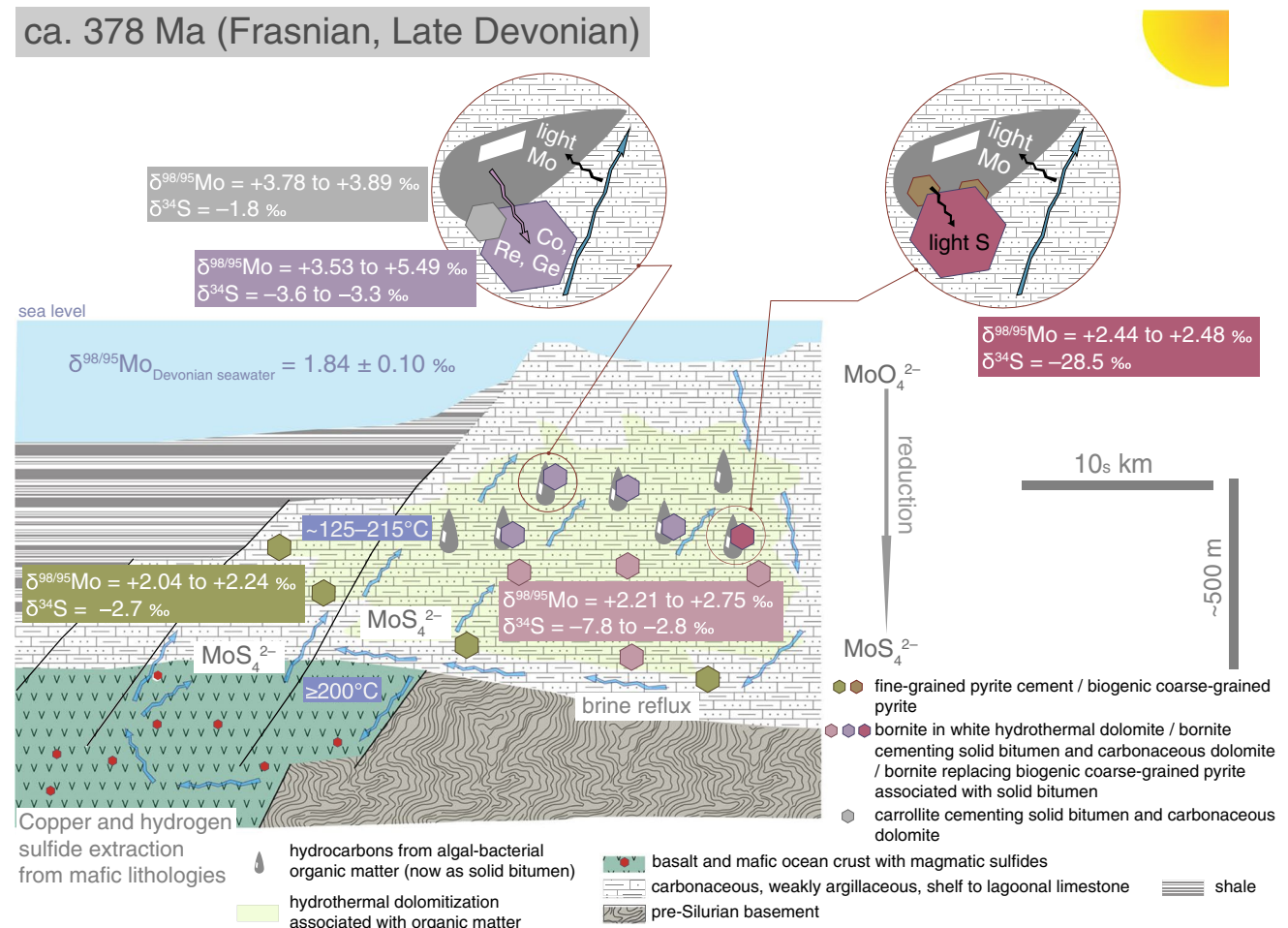


Fig. 4 Genetic model for epigenetic Cu-Co mineralization hosted in dolomitized Wenlock-Emsian carbonaceous limestone at Ruby Creek-Bornite in the Frasnian to Famennian

have contributed to the dynamics of flow of pulsed mineralizing fluids for sediment-hosted Cu-Co sulfide mineralization in reef-bearing carbonate platform.

Supplementary Information The online version contains supplementary material available at <https://doi.org/10.1007/s00126-022-01123-1>.

Acknowledgements N.J.S. thanks Profs. R.A. Creaser (University of Alberta) and D. Selby (Durham University) for mentoring during the setting up of the Re-Os isotope geochemistry and geochronology laboratory at ETH Zürich. We thank an anonymous reviewer, the Associate Editor D. Dolejš, and the Editor-in-Chief G. Beaudoin for their pertinent comments and suggestions on a previous version of this manuscript.

Author contribution Nicolas J. Saintilan (NJS) designed the study, carried out petrographic investigations, mineral separation, sulfide Re-Os isotope geochemistry procedures, and N-TIMS mass spectrometry analyses. Corey Archer and NJS carried out molybdenum isotope geochemistry and multi-collector mass spectrometry analyses on sulfide aliquots provided by NJS. Colin Maden helped NJS with setting up and tuning the thermal ionization mass spectrometer to negative mode for Re and Os mass spectrometry analyses. Elias Samankassou contributed

insights into the paleontology, paleogeography, and thermal evolution of the carbonate platform in the study area. Stefano M. Bernasconi and Jorge E. Spangenberg carried out sulfur mass spectrometry analyses on sulfide aliquots provided by NJS. According to guidelines provided by NJS for optimum samples selection for sulfide Re-Os geochronology, David Szumigala, Zach Mahaffey, and Andy West collected all samples from drill cores owned by Ambler Metals in Alaska. These authors provided the samples to NJS together with detailed background geological knowledge on the study area in the Cosmos Hills in Alaska. NJS wrote the manuscript and produced the figures. All co-authors read, commented and approved the final version of the manuscript.

Funding Open access funding provided by the Swiss Federal Institute of Technology (ETH) Zürich. This work was supported by an Ambizione Fellowship (PZ00P2_180133) of the Swiss National Science Foundation awarded to Nicolas J. Saintilan (N.J.S.).

Declarations

Conflict of interest The authors declare no competing interests.

Open Access This article is licensed under a Creative Commons Attribution 4.0 International License, which permits use, sharing,

adaptation, distribution and reproduction in any medium or format, as long as you give appropriate credit to the original author(s) and the source, provide a link to the Creative Commons licence, and indicate if changes were made. The images or other third party material in this article are included in the article's Creative Commons licence, unless indicated otherwise in a credit line to the material. If material is not included in the article's Creative Commons licence and your intended use is not permitted by statutory regulation or exceeds the permitted use, you will need to obtain permission directly from the copyright holder. To view a copy of this licence, visit <http://creativecommons.org/licenses/by/4.0/>.

References

- Algeo TJ, Scheckler SE (1998) Terrestrial-marine teleconnections in the Devonian: links between the evolution of land plants, weathering processes, and marine anoxic events. *Phil Trans Royal Soc London B* 353:113–130
- Andersson B, Godhe A, Filipsson HL, Rengefors K, Berglund O (2020) Differences in metal tolerance among strains, populations, and species of marine diatoms – importance of exponential growth for quantification. *Aquat Toxicol* 226:105551
- Bernstein LR, Cox DP (1986) Geology and sulfide mineralogy of the Number One orebody, Ruby Creek copper deposit. *Alaska Econ Geol* 81:1675–1689
- Brugger J, Hofmann M, Petri S, Feulner G (2019) On the sensitivity of the Devonian climate to continental configuration, vegetation cover, orbital configuration, CO₂ concentration, and insolation. *Paleocean Paleoclim* 34:1375–1398
- Chetty D, Frimmel HE (2000) The role of evaporites in the genesis of base metal sulfide mineralization in the Northern Platform of the Pan-African Damara Belt, Namibia: geochemical and fluid inclusion evidence from carbonate wall rock alteration. *Miner Deposita* 35:364–376
- Copper P, Scotese CR (2003) Megareefs in Middle Devonian super-greenhouse climates. *Geol Soc Amer Sp Paper* 370:209–230
- Davies GR, Smith LB (2006) Structurally controlled hydrothermal dolomite reservoir facies: an overview. *Amer Assoc Petrol Geol Bull* 90:1641–1690
- Demicco RV, Lowenstein T, Hardie LA, Spencer RJ (2005) Model of seawater composition for the Phanerozoic. *Geology* 33:877–880
- Falkowski P, Knoll AH (2011) Evolution of primary producers in the sea. *Academic Press*
- Gadd MG, Peter JM, Hnatyshin D, Creaser RA, Gouwy S, Fraser T (2020) A Middle Devonian basin-scale precious metal enrichment event across northern Yukon (Canada). *Geology* 46:242–246
- Gee DG, Janak M, Majka J, Robinson P, van Roermund H (2013) Subduction along and within the Baltoscandian margin during closure of the Iapetus Ocean and Baltica-Laurentia collision. *Lithosphere* 5:169–178
- Gordon GW, Lyons TW, Arnold GL, Roe J, Sageman BB, Anbar AD (2009) When do black shales tell molybdenum isotope tales? *Geology* 37:535–538
- Haq BU, Schutter SR (2008) A chronology of Paleozoic sea-level changes. *Science* 322:64–68
- Hawco NJ, McIlvin MM, Bundy RM, Tagliabue A, Goepfert TJ, Moran DM, Valentin-Alvarado L, DiTullio GR, Saito MA (2020) Minimal cobalt metabolism in the marine cyanobacterium *Prochlorococcus*. *Proc Natl Acad Science* 117:15740–15747
- Heijlen W, Banks DA, Muchez P, Stensgard BM, Yardley BWD (2008) The nature of mineralizing fluids of the Kipushi Zn-Cu deposit, Katanga, Democratic Republic of Congo: Quantitative fluid inclusion analysis using laser ablation ICP-MS and bulk crush-leach methods. *Econ Geol* 103:1459–1482
- Hitzman MW (1983) Geology of the Cosmos Hills and its relationship to the Ruby Creek copper-cobalt deposit. PhD dissert, Stanford University USA Unpub 266
- Hitzman MW (1986) Geology of the Ruby Creek copper deposit, Southwestern Brooks Range. *Alaska Econ Geol* 81:1644–1674
- Hitzman MW, Proffett JM, Schmidt J, Smith TE (1986) Geology and mineralization of the Ambler district, Northwestern Alaska. *Econ Geol* 81:1592–1618
- Hitzman MW, Selley D, Bull S (2010) Formation of sedimentary rock-hosted stratiform copper deposits through Earth history. *Econ Geol* 105:627–639
- Hoiland CW, Miller EL, Pease V, Hourigan JK (2017) Detrital zircon U-Pb geochronology and Hf isotope geochemistry of meta-sedimentary strata in the southern Brooks Range: constraints on Neoproterozoic-Cretaceous evolution of Arctic Alaska. *Geol. Soc. London. Sp Publ* 460:121–158
- Hoiland CW, Miller EL, Pease V (2018) Greenschist facies metamorphic zircon overgrowths as a constraint on exhumation of the Brooks Range metamorphic core, Alaska. *Tectonics* 37:3429–3455
- Intiomale MM, Oosterbosch R (1974) Géologie et géochimie du gisement de Kipushi, Zaïre, in Bartholom P (ed.) Gisements stratiformes et provinces cuprifères: Annales de la Société géologique de Belgique, Liège, Belgium, Centenaire de la Société Géologique de Belgique, 123–164
- Joachimski MM, Buggisch W (2003) Anoxic events in the late Frasnian – causes of the Frasnian-Famennian faunal crisis. *Geology* 21:675–678
- Joachimski MM, Breisig S, Buggisch W, Talent JA, Mawson R, Gereke M, Morrow JR, Day J, Weddige K (2009) Devonian climate and reef evolution: insights from oxygen isotopes in apatite. *Earth Planet Science Lett* 284:599–609
- Johnson JG, Klapper G, Sandberg CA (1985) Devonian eustatic fluctuations in Euramerica. *Geol Soc Amer Bull* 96:567–587
- Jones GD, Whitaker FF, Smart PL, Sanford WE (2002) Fate of reflux brines in carbonate platforms. *Geology* 30:371–374
- Kabanov P, Jiang C (2020) Photic-zone euxinia and anoxic events in a Middle-Late Devonian shelfal sea of Panthalassan continental margin, NW Canada: changing paradigm of Devonian ocean and sea level fluctuations. *Global Plat Change* 188:103153
- Kerl CF, Lohmayer R, Bura-Nakić E, Vance D, Planer-Friedrich B (2017) Experimental confirmation of isotope fractionation in thiomolybdates using ion chromatographic separation and detection by multicollector ICPMS. *Anal Chem* 89:3123–3129
- King EK, Perakis SS, Pett-Ridge J (2018) Molybdenum isotope fractionation during adsorption to organic matter. *Geochim Cosmochim Acta* 222:584–598
- Lenton TM, Dahl TW, Daines SJ, Mills BJW, Ozaki K, Saltzman MR, Porada P (2016) Earliest land plants created modern levels of atmospheric oxygen. *Proc Natl Acad Sci USA* 13:9704–9709
- Magnall JM, Gleeson SA, Poulton SW, Gordon GW, Paradis S (2018) Links between seawater paleoredox and the formation of sediment-hosted massive sulfide (SHMS) deposits – Fe speciation and Mo isotope constraints from Late Devonian mudstones. *Chem Geol* 490:45–60
- Mako DA, Shanks WC III (1984) Stratiform sulfide and barite-fluorite mineralization of the Vulcan prospect, Northwest Territories: exhalation of basinal brines along a faulted continental margin. *Can J Earth Sci* 21:78–91
- McClelland WC, Schmidt JM, Till AB (2006) New U-Pb SHRIMP ages from Devonian felsic volcanic and Proterozoic plutonic rocks of the southern Brooks Range, AK. *Geol Soc Amer Abstracts with Programs* 38:12
- Miller EL, Kuznetsov N, Soboleva A, Udoratina O, Grove MJ, Gehrels G (2011) Baltica in the Cordillera? *Geology* 39:791–794

- Morel FMM, Lam PJ, Saito MA (2020) Trace metal substitution in marine phytoplankton. *Annual Rev Earth Planet Sci* 48:491–517
- Peucker-Ehrenbrink B, Ravizza G (2000) The marine osmium isotope record. *Terra Nova* 12:205–219
- Racionero-Gómez B, Sproson AD, Selby D, Gröcke DR, Redden H, Greenwell HC (2016) Rhenium uptake and distribution in phaeophyceae macroalgae, *Fucus Vesiculosus*. *Royal Soc Open Sci* 3:160161
- Racionero-Gómez B, Sproson AD, Selby D, Gannoun A, Gröcke DR, Greenwell HC, Burton KW (2017) Osmium uptake, distribution, and $^{187}\text{Os}/^{188}\text{Os}$ and $^{187}\text{Re}/^{188}\text{Os}$ compositions in Phaeophyceae macroalgae, *Fucus vesiculosus*: Implications for determining the $^{187}\text{Os}/^{188}\text{Os}$ composition of seawater. *Geochim Cosmochim Acta* 199:48–57
- Rateman NS, McClelland WC, Presnell RD (2006) Geochronology and litho geochemistry of volcanic rocks of the Ambler district, southern Brooks Range, Alaska. *Geol Soc Amer Abstracts with Programs* 38:69
- Robinson FA, Toro J, Pease V (2019) U-Pb and oxygen isotope characteristics of Timanian- and Caledonian-age detrital zircons from the Brooks Range, Arctic Alaska. *USA Geol Soc Amer Bull* 131:1459–1479
- Rohr DM, Hoiland C, Blodgett RB (2018) A Silurian coelocaulid gastropod from Arctic Alaska and its paleogeographic significance. In: *Fossil Record 6*, Lucas SG, Sullivan RM (eds.). *New Mexico Mus Nat Hist Sci Bull* 79:585–587
- Runnells DD (1964) Cymrite in a copper deposit, Brooks Range, Alaska. *Am Mineral* 49:158–165
- Runnells DD (1965) Anthraxolite derived from indigenous organic matter in Middle Devonian dolomite, Cosmos Hills. *Alaska Jour Sed Petrol* 35:599–603
- Runnells DD (1969) The mineralogy and sulfur isotopes of the Ruby Creek copper prospect, Bornite. *Alaska Econ Geol* 64:75–90
- Ryb U, Erel Y, Matthews A, Avni Y, Gordon G, Anbar AD (2009) Large molybdenum isotope variations trace subsurface fluid migration along the Dead Sea transform. *Geology* 37:463–466
- Saintilan NJ, Selby D, Creaser RA, Dewaele S (2018) Sulfide Re-Os geochronology links orogenesis, salt and Cu-Co ores in the Central African Copperbelt. *Sci Rep* 8:14946
- Saintilan NJ, Selby D, Hughes JW, Schlatter D, Kolb J, Boyce A (2020) Mineral separation protocol for accurate and precise rhenium-osmium (Re-Os) geochronology and sulfur isotope composition of individual sulfide species. *MethodsX* 7:100944
- Saintilan NJ, Sproson AD, Selby D, Rottier B, Casanova V, Creaser RA, Kouzmanov K, Fontboté L, Piecha M, Gereke M, Zambito JJ IV (2021) Osmium isotopic constraints on sulfide formation in the epithermal environment of magmatic-hydrothermal mineral deposits. *Chem Geol* 564:120053
- Saintilan NJ, Bernasconi SM, Ikenne M, Toma J, Creaser RA, Souhassou M, Allaz JM, Karfal A, Maacha L, and Spangenberg JE (2022) Giant cobalt-nickel arsenide mineralization results from cold hydrocarbon seep and Upper Devonian brine circulation in Neoproterozoic serpentinite (Bou Azzer, Morocco). 16th Biennial Meeting of the Society for Geology Applied to Mineral Deposits, Rotorua, New Zealand, Proceedings with Abstracts
- Scott C, Lyons TW, Bekker A, Shen Y, Poulton SW, Chu X, Anbar AD (2008) Tracing the stepwise oxygenation of the Proterozoic ocean. *Nature* 452:456–459
- Selby D, Kelley KD, Hitzman MW, Zieg J (2009) Sulfide (bornite, chalcopyrite, and pyrite) systematics of the carbonate-hosted copper deposits at Ruby Creek, Southern Brooks Range. *Alaska Econ Geol* 104:437–444
- Shalev E, Yechieli Y (2007) The effect of Dead Sea level fluctuations on the discharge of thermal springs. *Isr J Earth Sci* 56:19–27
- Sim R, Davis BM, Austin JB (2022) Trilogy Metals Inc. NI 43–101 Technical Report on the Bornite Project, Northwest Alaska, USA. Open file report (<https://trilogymetals.com/news-and-media/news/trilogy-metals-files-technical-report-for-cobalt-resource-estimate-at-the-bornite-project>)
- Smith LB, Schieber J, Wilson RD (2019) Shallow-water onlap model for the deposition of Devonian black shales in New York, USA. *Geology* 47:279–283
- Smith LB, Schieber J, Wilson RD (2019) Shallow-water onlap model for the deposition of Devonian black shales in New York, USA – reply to ver Straeten et al. *Geology* 47:e496
- Spinks SC, Pearce MA, Liu W, Kunzmann M, Ryan CG, Moorhead GF, Kirkham R, Blaikie T, Sheldon HA, Schaub PM, Rickard WDA (2021) Carbonate replacement as the principal ore formation process in the Proterozoic McArthur River (HYC) sediment-hosted Zn-Pb deposit, Australia. *Econ Geol* 115:693–718
- Sutton JN, Ellwood MJ, Maher WA, Croot PL (2010) Oceanic distribution of inorganic germanium relative to silicon: germanium discrimination by diatoms. *Glob Biogeochem Cycles* 24:GB2017
- Till AB, Dumoulin JA, Harris AG, Moore TE, Bleick HA, Siwec BR (2008) Bedrock geologic map of the southern Brooks Range, Alaska, and accompanying conodont data. *US Geological Survey Open-File Report* 1149
- Tshileo PM, Walisumbu CS, Kaluendi K, Cailteux JL (2003) The Kipushi Zn-Pb-Cu deposit. *Guide-Book to the Field Trip, IGCP*. 450:210–3
- Turner EC, Broughton DW, Brooks T (2018) Neoproterozoic carbonate lithofacies and ore distribution at the Kipushi Cu-Zn deposit, Democratic Republic of Congo, and Gayna River Zn camp, Northwest Territories, Canada. *Econ Geol* 113:779–788
- Vasyukova OV, Williams-Jones AE (2022) Constraints on the genesis of cobalt deposits: Part II Applications to Natural Systems. *Econ Geol* 117:529–544
- Ver Straeten C, Brett C, Baird G, Boyer D, Lindemann R, Ivany L, Over DJ, Witzke B (2019) Shallow-water onlap model for the deposition of Devonian black shales in New York, USA – Comment. *Geology* 47:e495
- Voegelin AR, Nägler TF, Pettke T, Neubert N, Steinmann M, Pourret O, Villa IM (2012) The impact of igneous bedrock weathering on the Mo isotopic composition of stream waters: Natural samples and laboratory experiments. *Geochim Cosmochim Acta* 86:150–165
- Wallace MW, Hood AvS, Shuster A, Greig A, Planavsky NJ, Reed CP (2017) Oxygenation history of the Neoproterozoic to early Phanerozoic and the rise of land plants. *Earth Planet Sci Lett* 466:12–19
- Wilkinson JJ, Everett CE, Boyce AJ, Gleeson SA, Rye DM (2005) Intracratonic crustal seawater circulation and the genesis of sub-seafloor zinc-lead mineralization in the Irish orefield. *Geology* 33:805–808
- Witzke BJ (2011) Estimating magnitudes of sea-level changes associated with Middle and Upper Devonian sequences in the Iowa area: *Geological Society of America Abstracts with Program* 43:96
- Zhong R, Brugger J, Chen Y, Li W (2015) Contrasting regimes of Cu, Zn, and Pb transport in ore-forming hydrothermal fluids. *Chem Geol* 395:154–164

Publisher's note Springer Nature remains neutral with regard to jurisdictional claims in published maps and institutional affiliations.